Atmos. Chem. Phys. Discuss., https://doi.org/10.5194/acp-2017-319
Manuscript under review for journal Atmos. Chem. Phys.
Discussion started: 23 June 2017

Atmospheric Chemistry and Physics Discussions

Future threat to boreal ecosystem health from wildfire air pollution

Xu Yue[1], Susanna Strada[2], Nadine Unger[3]

[1] Climate Change Research Center, Institute of Atmospheric Physics, Chinese Academy of Sciences, Beijing 100029, China
[2] Laboratoire des Sciences du Climat et de l'Environnement, L'Orme des Merisiers - Bat 712, 91191 Gif Sur Yvette, France
[3] College of Engineering, Mathematics and Physical Sciences, University of Exeter, Exeter, EX4 4QE, UK

Corresponding author:
Xu Yue
Telephone: 86-10-82995369
Email: xuyueseas@gmail.com

Keywords: wildfire emissions, ozone, aerosols, net primary productivity, climate change, diffuse fertilization effect, carbon loss, earth system modeling

Atmos. Chem. Phys. Discuss., https://doi.org/10.5194/acp-2017-319
Manuscript under review for journal Atmos. Chem. Phys.
Discussion started: 23 June 2017

Atmospheric Chemistry and Physics Discussions

Abstract

Biomass burning is an important source of tropospheric ozone (O_3) and aerosols. These air pollutants can affect vegetation photosynthesis through stomatal uptake (for O_3) and light scattering (for aerosols). Climate change will significantly increase wildfire activity in boreal North America by the midcentury, while little is known about the impacts of enhanced emissions on the terrestrial carbon budget. Here, combining site-level and satellite observations and a carbon-chemistry-climate model, we estimate the impacts of fire emitted O_3 and aerosols on net primary productivity (NPP) over boreal North America. Fire emissions are calculated based on an ensemble projection from 13 climate models. In the present day, wildfire enhances surface O_3 by 2 ppbv (7%) and aerosol optical depth (AOD) at 550 nm by 0.03 (26%) in the summer. By midcentury, boreal area burned is predicted to increase by 66%, contributing more O_3 (13%) and aerosols (37%). Fire O_3 causes negligible impacts on NPP because ambient O_3 concentration is far below the damage threshold of 40 ppbv. Fire aerosols reduce surface solar radiation but enhance atmospheric absorption, resulting in enhanced air stability and intensified regional drought. The domain of this drying is confined to the North in the present day, but extends southward by 2050 due to increased fire emissions. Consequently, wildfire aerosols enhance NPP by 72 Tg C yr^{-1} in the present day but decrease NPP by 118 Tg C yr^{-1} in the future, mainly because of the soil moisture perturbations. Our results suggest that future wildfire may accelerate boreal carbon loss, not only through direct emissions, but also through the biophysical impacts of fire aerosols.

Atmos. Chem. Phys. Discuss., https://doi.org/10.5194/acp-2017-319
Manuscript under review for journal Atmos. Chem. Phys.
Discussion started: 23 June 2017

Atmospheric Chemistry and Physics Discussions

1 Introduction

Wildfire is becoming more active in recent decades over North America boreal regions (Stocks et al., 2002; Kasischke and Turetsky, 2006). Fire activity is closely related to weather conditions and large-scale atmospheric oscillations (Gillett et al., 2004; Duffy et al., 2005), and is projected to increase significantly in the future due to climatic changes (Flannigan et al., 2005; Balshi et al., 2009). More frequent wildfires are accelerating carbon loss in boreal North America (Bond-Lamberty et al., 2007; Turetsky et al., 2011). Meanwhile, fire-induced air pollution, including ozone (O_3) and aerosols, is predicted to increase in boreal and downwind regions by midcentury (Yue et al., 2013; Yue et al., 2015). Wildfire emissions have large impacts on air quality (Wotawa and Trainer, 2000; Morris et al., 2006), weather/climate conditions (Randerson et al., 2006; Zhao et al., 2014), and public health (Zu et al., 2016; Liu et al., 2017). However, little is known about how these pollutants affect ecosystem carbon assimilation, and how this impact will change with the increased wildfire activity in the future.

Surface O_3 is detrimental to plant health because it damages photosynthesis through stomatal uptake (Sitch et al., 2007). In the present climate state, fire-induced O_3 enhancements are predicted to reduce net primary productivity (NPP) in the Amazon forest by 230 Tg C yr^{-1}, a magnitude comparable to the direct release of CO_2 from fires in South America (Pacifico et al., 2015). The aerosol effects are more uncertain because both positive and negative feedbacks occur. Appearance of aerosols increases diffuse light, which is beneficial for shaded leaves in the lower canopy. Consequently, photosynthesis of the whole ecosystem will increase as long as the total light availability is not compromised (Kanniah et al., 2012). Rap et al. (2015) estimated that biomass burning aerosols increase Amazon NPP by 78–156 Tg C yr^{-1}, which offsets about half of the damage caused by fire O_3 (Pacifico et al., 2015). In contrast, strong light attenuation associated with high aerosol loading may decrease canopy photosynthesis (Cohan et al., 2002; Oliveira et al., 2007; Cirino et al., 2014). Furthermore, the aerosol radiation changes indirectly influence land carbon uptake through concomitant meteorological perturbations that are only beginning to be examined (Yue et al., 2017).

Future wildfire activity is projected to increase over boreal North America but with large uncertainties (Flannigan et al., 2005; Tymstra et al., 2007; Girardin and Mudelsee, 2008; Nitschke and Innes, 2008; Amiro et al., 2009; Balshi et al., 2009; Bergeron et al., 2010;

Wotton et al., 2010; de Groot et al., 2013; Wang et al., 2016). For example, Amiro et al. (2009) predicted an increase of 34% in Canadian area burned for a 2×CO_2 scenario (2040-2060) relative to a 1×CO_2 condition (1975-1995), using the Canadian Fire Weather Index (CFWI) and output from Canadian global climate model (CGCM) version 1. On the other hand, Balshi et al. (2009) projected that area burned in boreal North America would double by the year 2045-2050 relative to 1991-2000, using the Multivariate Adaptive Regression Splines (MARS) approach and meteorological output from CGCM version 2. The increasing rate in Balshi et al. (2009) is higher than that in Amiro et al. (2009), indicating substantial uncertainties in fire projections originating from both fire models and simulated future climate. Recently, Yue et al. (2015) developed stepwise regressions over boreal ecoregions between area burned and multiple meteorological variables as well as CFWI indexes. They used output from 13 climate models to drive these regression models and predicted an average increase of 66% in boreal area burned at 2046-2065 relative to 1981-2000 under the IPCC A1B scenario (Solomon et al., 2007). The multi-model ensemble projection reduces uncertainties associated with single model climate projections. Yue et al. (2015) calculated that the wildfire emission increase by the 2050s would increase mean summertime surface O_3 by 5 ppbv in Alaska and 3 ppbv in Canada. The study found regional maximum O_3 enhancements as high as 15 ppbv, suggesting the potential for possible vegetation damage and land carbon loss due to the enhanced boreal fire-related air pollution. Wildfire aerosols are also expected to increase significantly but not predicted in Yue et al. (2015).

In this study, we quantify the impacts of O_3 and aerosols emitted from boreal wildfires on the land carbon uptake in North America in the present climate state and in the future world at 2050, taking advantage of the ensemble projection of future wildfire emissions by Yue et al. (2015). We first analyze relationships between gross primary production (GPP) and aerosol optical depth (AOD) at 550 nm over the boreal regions based on observations. We then perform a suite of Earth system model simulations using NASA GISS ModelE2 that embeds the Yale Interactive Terrestrial Biosphere model (YIBs), a framework known as ModelE2-YIBs (Yue and Unger, 2015). Future projections of wildfire emissions from Yue et al. (2015) are applied as input to ModelE2-YIBs model to project fire-induced O_3 and aerosol concentrations in the 2010s and 2050s. The impacts of the boreal fire O_3 on forest photosynthesis are predicted using the flux-based damage algorithm proposed by Sitch et al. (2007). Fire aerosols induce perturbations to radiation, meteorology, and hydrology, leading to multiple influences on the land carbon uptake. Sensitivity experiments are performed using

the YIBs model in offline mode to isolate the contributions of changes in the individual meteorological drivers.

2 Materials and methods

2.1 Observed GPP-AOD relationships

Following the approach by Strada et al. (2015), we investigate the GPP sensitivity to diffuse radiation and AOD variability in boreal regions. First, we identify study sites in Canada and Alaska from the AmeriFlux (AMF) network (http://ameriflux.lbl.gov/). The number of available boreal sites is much fewer than those in temperate regions. We select AMF sites providing hourly (or half-hourly) simultaneous measurements of GPP (non gap-filled) and photosynthetically active radiation (PAR, total and diffuse) for at least 3 consecutive years. Only two Canadian sites meet the criteria: Groundhog River (CA-Gro, 82.2°W, 48.2°N), a mixed forest (MF), and Quebec Mature Boreal Forest Site (CA-Qfo, 73.4°W, 49.7°N), an evergreen needleleaf forest (ENF). At the two selected sites, we calculate the Pearson's correlation coefficients between half-hourly GPP and different components of PAR. We then apply instantaneous Level 2 Collection 6 of AOD pixels at 3-km resolution retrieved by the Moderate Resolution Imaging Spectroradiometer (MODIS, https://ladsweb.nascom.nasa.gov/) onboard the Aqua and Terra satellites (Levy et al., 2013). The MODIS 3-km AOD product has been fully validated against ground-based sun photometers at both global (Remer et al., 2013) and urban/suburban (Munchak et al., 2013) scales. Strada et al. (2015) used ground-based AOD observations from the Aerosol Robotic Network (AERONET) near AMF sites to validate the sampling technique of MODIS 3-km AOD product. For this study, the validation against ground-based AOD observations was not possible because no AERONET stations exist near to the selected AMF sites.

Every day, MODIS satellite sensors pass a specific region between 10:00 and 14:00 Local Time (LT), leaving patchy signals around the AmeriFlux sites. Most of MODIS AOD data at high latitudes are available only in boreal summer; as a result, we narrow our explorations of the GPP-AOD relationships to the noontime (10:00-14:00 LT) from June to August. The chosen noontime window limits the contributions that confounding factors such as low solar angles and high diffuse fraction may have on the amount of diffuse PAR and plant

productivity (Niyogi et al., 2004). For each summer day, we select instantaneous MODIS 3-km AOD pixels that are (a) located within a distance of 0.03° (about 3 km) from the targeted AMF site and (b) "quasi-coincident" with AMF data, which are available each half-hour. Because of the unavoidable temporal differences between MODIS overpass and AMF data availability, we name this selection "quasi-coincident". Cloud mask, applied in the MODIS retrieval procedure, conveniently filters out cloudy instants and should reduce the effect of clouds in the scattering process. We calculate both the correlation and regression coefficients between "quasi-coincident" GPP and AOD at the selected sites. Negative GPP is considered as a missing value. To further reduce the influence of cloud cover, we discard instants (both AMF and MODIS data) when precipitation is non-zero. The GPP-AOD sampling pairs are much fewer than GPP-PAR, because we select instants when both instantaneous AOD and GPP data are available. In addition, AOD is screened for clear instants to exclude the impacts of clouds.

2.2 Wildfire emissions

Wildfire emissions used in climate modeling are calculated as the product of area burned, fuel consumption, and emission factors. To predict area burned, we build stepwise regressions for area burned in 12 boreal ecoregions (Yue et al., 2015). Observed area burned aggregated from inter-agency fire reports is used as the predictand. Predictors are selected from 44 (5×6+7×2) variables including five meteorological parameters (mean and maximum temperature, relative humidity, precipitation, and geopotential height at 500 hPa) of six different time intervals (winter, spring, summer, autumn, fire season (May-October), and the whole year), as well as the mean and maximum values of 7 fire indexes from the CFWI system during fire season. We consider the impacts of antecedent factors on current fire activity by including all above variables at the same year and those in the previous two years, making a total of 132 (44×3) factors. The final formats of regression are different among ecoregions, depending on the selection of the factors that contribute the maximum observed variance in predictand but remain the minimum collinearity among predictors. These regression functions are then driven with output from 13 CMIP3 climate models (Meehl et al., 2007) to predict area burned at present day (1981-2000) and midcentury (2046-2065).

Fuel consumption, the dry mass burned per fire area, is the product of fuel load and burning severity. For fuel load in Alaska, we use 1-km inventory from the US Forest Service (USFS)

Atmos. Chem. Phys. Discuss., https://doi.org/10.5194/acp-2017-319
Manuscript under review for journal Atmos. Chem. Phys.
Discussion started: 23 June 2017

Atmospheric Chemistry and Physics Discussions

Fuel Characteristic Classification System (FCCS, McKenzie et al., 2007). For fuel load in Canada, we use a 1-km fuel type map from the Canadian Fire Behavior Prediction (FBP) system (Nadeau et al., 2005), combined with fuel-bed definition from the FCCS. Burning severity, the fraction of fuel load burned by fires, is calculated with the USFS CONSUME model 3.0 following the approach described in Val Martin et al. (2012). With both fuel load and burning severity, we derive fuel consumption and further calculate biomass burned in boreal North America with the predicted area burned. Fire emissions for a specific species are then estimated as the product between biomass burned and the corresponding emission factor, which is adopted from measurements by Andreae and Merlet (2001) except for NO_x. We use the average values from six studies as NO_x emission factor, because the number reported in Andreae and Merlet (2001) is much higher than field observations (Alvarado et al., 2010). Based on projected area burned and observation-based fuel consumption and emission factors, we derive fire emissions of NO_x, carbon monoxide (CO), non-methane volatile organic compounds (NMVOCs, Alkenes and Alkanes), NH_3, SO_2, black (BC) and organic carbon (OC) in the present day and midcentury.

2.3 NASA ModelE2-YIBs model

The NASA ModelE2-YIBs is an interactive climate-carbon-chemistry model, which couples the chemistry-climate model NASA ModelE2 (Schmidt et al., 2014) and the YIBs vegetation model (Yue and Unger, 2015). NASA ModelE2 is a general circulation model with horizontal resolution of 2°×2.5° latitude by longitude and 40 vertical layers up to 0.1 hPa. It dynamically simulates both the physical (emissions, transport, and deposition) and chemical (production, conversion, and loss) processes of gas-phase chemistry (NO_x, HO_x, O_x, CO, CH_4, and NMVOCs), aerosols (sulfate, nitrate, ammonium, BC, OC, dust, and sea salt), and their interactions. In the model, oxidants influence the photochemical formation of secondary aerosol species (e.g., sulfate, nitrate, and biogenic secondary organic aerosol), in turn, aerosols alter photolysis rates and influence the online gas-phase chemistry. The model also considers interactions between climate and atmospheric components. Simulated climate affects formation, transport, and deposition of atmospheric components, in turn, both O_3 and aerosols influence climate by altering radiation, temperature, precipitation, and other climatic variables. Both observation-based evaluations and multi-model inter-comparisons indicate that ModelE2 demonstrates skill in simulating climatology (Schmidt et al., 2014), radiation

(Wild et al., 2013), atmospheric composition (Shindell et al., 2013b), and radiative effects (Shindell et al., 2013a).

YIBs is a process-based vegetation model that dynamically simulates changes in leaf area index (LAI) through carbon assimilation, respiration, and allocation. Coupled photosynthesis-stomatal conductance is simulated with the Farquhar-Ball-Berry scheme (Farquhar et al., 1980; Ball et al., 1987). Leaf-level photosynthesis is upscaled to canopy level by separating diffuse and direct light for sunlit and shaded leaves (Spitters, 1986). Plant respiration considers thermal dependence as well as acclimation to temperature (Atkin and Tjoelker, 2003). Soil respiration is calculated based on the carbon flows among 12 biogeochemical pools (Schaefer et al., 2008). Net carbon uptake is allocated among leaves, stems, and roots to support leaf development and plant growth (Cox, 2001). An interactive flux-based O_3 damage scheme proposed by Sitch et al. (2007) is applied to quantify the photosynthetic responses to ambient O_3 (Yue and Unger, 2014). The YIBs model has been benchmarked against *in situ* GPP from 145 eddy covariance flux tower sites and satellite retrievals of LAI and phenology (Yue and Unger, 2015).

2.4 Simulations

We perform 6 time-slice simulations, three for present-day (2010s) and three for midcentury (2050s), with atmosphere-only configuration to explore the impacts of fire emissions on NPP in boreal North America (Table 1). Simulations F10CTRL and F50CTRL turn off all fire emissions as well as O_3 vegetation damage for the 2010s and 2050s, respectively. However, climatic feedbacks of aerosols from other sources (both natural and anthropogenic) and related photosynthetic responses are included. Simulations F10AERO and F50AERO consider the responses of plant productivity to perturbations in radiation and meteorology caused by aerosols, including emissions from wildfires and other sources, but do not include any O_3 vegetation damage. In contrast, simulations F10O3 and F50O3 calculate offline O_3 damage based on the simulated O_3 from all sources including fire emissions. Vegetation NPP, the net carbon uptake by biosphere, is the impact metric. The difference between AERO and CTRL runs isolates the impacts of fire aerosols on NPP, and the difference between O3 and CTRL runs isolates O_3 vegetation damage caused by fire and non-fire emission sources.

Atmos. Chem. Phys. Discuss., https://doi.org/10.5194/acp-2017-319
Manuscript under review for journal Atmos. Chem. Phys.
Discussion started: 23 June 2017

Atmospheric Chemistry and Physics Discussions

All simulations are conducted for 20 years and outputs for the last 15 years are used for analyses. The simulations apply sea surface temperatures (SSTs) and sea ice distributions from previous NASA GISS experiments under the IPCC RCP8.5 scenario (van Vuuren et al., 2011) archived for the Coupled Model Intercomparison Project Phase 5 (CMIP5). Decadal average monthly-varying SST and sea ice of 2006-2015 are used as boundary conditions for present-day (2010s) runs while that of 2046-2055 are used for future (2050s) runs. Decadal average well-mixed greenhouse gas concentrations and anthropogenic emissions of short-lived species, both at present day and midcentury, are adopted from the RCP8.5 scenario (Table 2). Natural emissions of soil and lightning NO_x, biogenic volatile organic compounds (BVOC), dust, and sea salt are climate-sensitive and simulated interactively. The RCP8.5 land cover change dataset shows limited changes in land cover fractions between 2010s and 2050s (Oleson et al., 2010). For example, relative to the 2010s, a maximum gain of 5% is predicted for grassland in the 2050s, resulting from a 1% loss in deciduous forest and another 1% loss in needleleaf forest over boreal North America. As a result, a land cover dataset derived from satellite retrievals (Hansen et al., 2003) is applied for both the 2010s and 2050s.

To isolate the impact of individual aerosol-induced climatic perturbations on NPP, we perform 10 sensitivity experiments using the YIBs vegetation model driven with offline meteorology simulated by ModelE2-YIBs model (Table 3). For example, the offline run Y10_CTRL is driven with variables from the online simulation of F10CTRL (Table 1). The run Y10_TAS adopts the same forcing as Y10_CTRL except for temperature, which is simulated by the climate simulation of F10AERO. In this case, we quantify the NPP responses to individual and/or combined climate feedback (mainly in temperature, radiation, and soil moisture) by fire aerosols. Each offline run is conducted for 12 years and the last 10 years are used for analyses.

2.5 Observation datasets

We use observations to evaluated GPP, AOD, and O_3 in boreal North America simulated by ModelE2-YIBs. For GPP, we use a benchmark data product upscaled from FLUXNET eddy covariance data using an ensemble of regression trees (Jung et al., 2009). For AOD observations, we use satellite retrieval at 550 nm from Terra MODIS Level 3 data product. For O_3, gridded datasets are not available. We use site-level observations from 81 U.S. sites at the Clean Air Status and Trends Network (CASTNET, https://www.epa.gov/castnet) and

202 Canadian sites at the National Air Pollution Surveillance (NAPS, http://www.ec.gc.ca/rnspa-naps/) program. All datasets are averaged over the 2008-2012 period to represent present-day climatological conditions. Gridded datasets are interpolated to the same 2°×2.5° resolution as ModelE2-YIBs model.

3 Results

3.1 Observed GPP-AOD relationships

Positive correlations between GPP and diffuse PAR are found at the two boreal sites (Figs 1b-1c). The magnitude of diffuse PAR is similar for these sites, possibly because they are located at similar latitudes (Fig. 1a). GPP values at CA-Gro are generally higher than that at CA-Qfo, likely because deciduous broadleaf forest (DBF) has higher photosynthetic rates. Consequently, the slope of regression between GPP and PAR_{dif} is higher at CA-Gro than that at CA-Qfo, suggesting that GPP of DBF (or MF) is more sensitive to changes in diffuse PAR than that of ENF. We find almost zero correlation between GPP and PAR_{dir} at the two sites (Table 4), indicating that photosynthesis is in general light-saturated for sunlit leaves at these sites during boreal summer noontime. As a result, modest reductions in direct light by aerosols will not decrease GPP of the whole canopy.

With satellite-based AOD, we find positive correlations between GPP and AOD at both sites (Figs 1d-1e). However, the slope of regression between GPP and AOD is lower at CA-Gro compared with that at CA-Qfo, opposite to the GPP-PAR_{dif} regressions. The cause of such discrepancy might be related to the limitation of data availability. For the same reason, the GPP-AOD correlation is insignificant at CA-Gro site. On average, we estimate GPP sensitivity of 3.5 ± 1.1 μmol m^{-2} s^{-1} per unit AOD at lower latitudes of boreal regions in the summer.

3.2 Evaluation of model photosynthesis and atmospheric composition

Simulated summer GPP shows high values in mid-western Canada (Alberta and Saskatchewan) and the Southeast (Ontario) (Fig. 2a). Forest GPP at high latitudes is low because of the cool weather and light limitation there. Compared against the data product,

simulated GPP reasonably captures the spatial distribution with a high correlation coefficient of 0.77 ($p << 0.01$) and relatively small biases within 20%. Simulated AOD reproduces the observed spatial pattern including the high values in boreal forests (Fig. 2b). In contrast to the MODIS observations, predicted AOD is relatively uniform over the West with a background value of ~0.1. This discrepancy explains the low correlation coefficient (R = 0.25, p<0.01) between the model and MODIS data. Simulated [O_3] shows low values in boreal North America and high values in the western and eastern U.S. (Fig. 3a). This pattern is consistent with surface observations (Fig. 3b), but the model overestimates the measured surface O_3 by 40%. The Canadian measurement sites are located near the southern boundary, and as a result do not represent the average state over the vast boreal region at higher latitudes.

3.3 Simulation of wildfire O_3 and aerosols

Compared to the present day, wildfire area burned is projected to increase by 66% in boreal North America at midcentury, mainly because of the higher temperature in future fire seasons (Yue et al., 2015). Consequently, enhanced fire emissions increase concentrations of surface O_3 and column AOD, especially over Alaska and central Canada (Fig. 4). The maximum centers of air pollutants are collocated for O_3 and AOD but with unproportional magnitudes, suggesting non-linear conversion among fire emission species as well as the interactions with natural emission sources (e.g., lightning/soil NO_x and BVOC). On average, wildfire emissions contribute 7.1 ± 3.1% to surface O_3 and 25.7 ± 2.4% to AOD in the summer over boreal North America in the present day. By midcentury, these ratios increase significantly to 12.8 ± 2.8% for O_3 and 36.7 ± 2.0% for AOD.

3.4 Simulation of fire pollution impacts on NPP

Surface O_3, including both fire and non-fire emissions (Table 2), causes limited damages to summer GPP in boreal North America (Fig. 5). The most significant damage is predicted over eastern U.S., where observed [O_3] is high over vast forest ecosystems (Fig. 3). In the western U.S., [O_3] is also high but the O_3-induced GPP reduction is trivial because low stomatal conductance in the semi-arid ecosystems limits O_3 uptake there (Yue and Unger, 2014). Over boreal regions, the mean [O_3] of 28 ppbv is much lower than the damaging threshold of 40 ppbv for most tree species (Yue et al., 2016). Statistics in Yue et al. (2015) show that maximum daily 8-hour average (MDA8) [O_3] can be higher than 40 ppbv in Alaska

and Canada. However, such episodes appear at 95 percentile for present day and 90 percentile for midcentury, suggesting that O_3 vegetation damage is rare in boreal North America and fire-induced O_3 enhancement does not exacerbate such damages. Therefore, we do not consider O_3 damage effects further.

Fire aerosols cause significant perturbations in shortwave radiation at surface (Fig. 6). The direct light is largely attenuated especially over Alaska and central Canada, where fire aerosols are most abundant (Fig. 4). In contrast, diffuse light widely increases due to particle scattering. In the present day, the average reduction of 5.6 W m^{-2} in the direct light component is in part offset by the enhancement of 2.6 W m^{-2} in the diffuse light component, leading to a net reduction of 3.0 W m^{-2} in solar radiation over boreal North America. By the midcentury, a stronger reduction of 9.5 W m^{-2} in direct light is accompanied by an increase of 4.0 W m^{-2} in diffuse light, resulting in a net reduction of 5.5 W m^{-2} in solar radiation. Fire-induced BC aerosols strongly absorb solar radiation in the atmospheric column (Figs 7a-7b). On average, fire aerosols absorb 1.5 W m^{-2} in the present day and 2.6 W m^{-2} by the midcentury.

Atmospheric circulation patterns respond to the aerosol-induced radiative perturbations (Figs 7c-7d). Surface radiative cooling and atmospheric heating together increase air stability and induce anomalous subsidence. In the present day, such descending motion is confined to 55-68°N, accompanied by a rising motion at 52-55°N (Fig. 7c). As a result, fire aerosols induce surface warming at higher latitudes but cooling at lower latitudes in boreal regions (Fig. 8a). Meanwhile, precipitation is inhibited by the subsidence in northwestern Canada but is promoted by the rising motion in the Southwest (Fig. 8c). By the midcentury, the range of subsidence expands southward to 42°N (Fig. 7d) due to strengthened atmospheric heating (Fig. 7b). The downward convection of warm air offsets surface radiative cooling (Fig. 6b), leading to a significant warming in the Southwest (Fig. 8b). The expanded subsidence further inhibits precipitation in vast domain of Canada (Fig. 8d). Soil moisture is closely related to rainfall and as a result exhibits dipole changes (drier north and wetter south) in the present day (Fig. 8e) but widespread reductions (Fig. 8f) by the midcentury.

In response to the climatic effects of fire aerosols, boreal NPP shows distinct changes between the present day and midcentury (Fig. 9). In the 2010s, forest NPP increases by 5-15% in Alaska and southern Canada, but decreases by 5-10% in northern and eastern Canada. This

pattern of NPP changes (ΔNPP) is connected to the climatic effects of aerosols, especially changes in soil moisture (Fig. 8). The correlation between ΔNPP (Fig. 9a) and changes in soil moisture (Fig. 8e) reaches R = 0.56 (n = 356), much higher than the values of R = -0.11 for temperature change (Fig. 8a) and R = 0.22 for precipitation change (Fig. 8c). At the continental scale, the patchy responses of NPP offset each other. Since the dominant fraction of carbon uptake occurs in southern Canada (Fig. 2a), where positive NPP change is predicted (Fig. 9a), wildfire aerosols enhance the total NPP by 72 Tg C yr^{-1} in the present day (Table 5). In contrast, increased wildfire emissions in the 2050s inhibit precipitation and decrease soil moisture in boreal North America (Fig. 8), leading to widespread NPP reductions and a total NPP loss of 118 Tg C yr^{-1} (Fig. 9b, Table 5).

4 Discussion

4.1 Roles of aerosol climatic feedback

The contrasting sign of NPP responses in the present day and midcentury are closely related to the aerosol-induced surface climatic feedback. Sensitivity experiments using offline YIBs model (Table 3) allowed assessment of the impacts of individual changes in the major meteorological drivers, including temperature, radiation (diffuse and direct), and soil moisture (Table 5). The offline simulations driven with changes in all three variables yield ΔNPP of 126 Tg C yr^{-1} for the 2010s and -97 Tg C yr^{-1} for the 2050s. These values are different from the online simulations, which predict ΔNPP of 72 Tg C yr^{-1} for the 2010s and -118 Tg C yr^{-1} for the 2050s. Missing of other aerosol climatic feedbacks in the offline model, for example, changes in relative humidity, surface pressure, soil temperature, and turbulence momentum, may cause such discrepancy between the online and offline simulations. Seasonal analyses show that summertime ΔNPP is 99 Tg C at present day and -95 Tg C at midcentury, dominating the NPP changes all through the year, because both wildfire emissions and ecosystem photosynthesis maximize in boreal summer.

Observations show that aerosols can promote plant photosynthesis through increasing diffuse radiation (Niyogi et al., 2004; Cirino et al., 2014; Strada et al., 2015). Our analyses with ground and satellite data also show positive correlations between GPP and AOD (Fig. 1). Wildfire aerosols enhance diffuse radiation by 2.6 W m^{-2} (1.7%) at present day and 4.0 W m^{-2}

(2.3%) at midcentury in boreal North America (Fig. 6). With these changes, simulated NPP increases by 8 Tg C yr^{-1} at the 2010s and 14 Tg C yr^{-1} at the 2050s (Table 5). Near the two AmeriFlux sites (Fig. 1a), wildfires increase local AOD by 0.03 (Fig. 4c). Meanwhile, we estimate that summer average (00:00-24:00) GPP increases by 0.04 μmol m^{-2} s^{-1} in the same region due to aerosol diffuse fertilization effects (DFE) based on the results of (Y10_PAR – Y10_CTRL). This change suggests a simulated GPP sensitivity of 1.2 μmol m^{-2} s^{-1} (22%) per unit AOD. Observed GPP sensitivity to AOD at the two sites are 2.3 (19%) and 4.5 μmol m^{-2} s^{-1} (58%) per unit AOD, respectively (Figs 1d-e). The absolute value of GPP sensitivity from simulations is much smaller than that of observations, because the former is for 24-h average while the latter is only for noontime (10:00-14:00). The relative change of 22% in YIBs model falls within the observed range of 19-58%.

The estimated NPP changes of 8 Tg C yr^{-1} by the radiative effects of boreal fire aerosols are much weaker than the enhancement of 78-156 Tg C yr^{-1} by fires in Amazon basin (Rap et al., 2015). There are at least two reasons for such discrepancies in the DFE between boreal and Amazon fire aerosols. First, wildfire emissions and associated impacts on radiation are much smaller in boreal regions. Wildfires in Alaska and Canada directly emit 68 Tg C yr^{-1} at the 2010s, resulting in enhancement of summer AOD by 35% and diffuse radiation by 1.7%. These boreal emissions are much smaller than the ~240 Tg C yr^{-1} in Amazon basin (van der Werf et al., 2010), where fires enhances regional PM2.5 concentrations by 85% and diffuse radiation by 6.2% in dry seasons (Rap et al., 2015). Second, larger solar insolation in lower latitudes allows stronger DFE for the same unit change of diffuse radiation. In our prediction, most of NPP changes occur at high latitudes of boreal regions (Fig. 9), where total insolation is not so abundant as that at the tropical areas. Consequently, decline of direct radiation in boreal regions more likely converts the light availability of sunlit leaves from light-saturation to light-limitation, offsetting the benefit from enhanced diffuse radiation for shaded leaves. For this study, we do not find GPP reduction by the decline of direct light at the two Ameriflux sites (Table 4), possibly because these sites are located at middle latitudes (<50°N). In the future, more observations at higher latitudes (> 55°N) are required to explore the sensitivity of GPP to AOD at the light-limited conditions.

Simulations have shown that absorbing aerosols can cause regional drought by increasing air stability (Liu, 2005; Cook et al., 2009; Tosca et al., 2010). Our results confirm such tendency but with varied range of hydrological responses depending on the magnitude of wildfire

454 emissions (Figs 8c-8f). Observations suggest that precipitation (and the associated soil
455 moisture) is the dominant driver of the changes in GPP over North America, especially for
456 the domain of cropland (Beer et al., 2010). Sensitivity experiments with offline YIBs model
457 show that changes in soil moisture account for 82.5% of ΔNPP at present day and 70.5% of
458 ΔNPP at midcentury (Table 5). These results suggest that aerosol-induced changes in soil
459 water availability, instead of temperature and radiation, dominantly contribute to the changes
460 of boreal NPP, consistent with observational and experimental results (Ma et al., 2012;
461 Girardin et al., 2016; Chen et al., 2017).
462
463 **4.2 Limitations and uncertainties**
464
465 For this study, we use the ensemble projected fire emissions from Yue et al. (2015). Area
466 burned is predicted based on the simulated meteorology from multiple climate models. Such
467 an approach may help reduce model uncertainties in climatic responses to CO_2 changes, but
468 cannot remove the possible biases in the selection of climate scenarios and fire models. All
469 predictions in Yue et al. (2015) are performed under the IPCC A1B scenario. With two
470 different scenarios, A2 of high emissions and B2 of low emissions, Balshi et al. (2009)
471 showed that future area burned in boreal North America increases at a similar rate until the
472 2050s, after which area burned in A2 scenario increases much faster than that in B2 scenario.
473 On average, boreal area burned in Balshi et al. (2009) increases by ~160% at 2051-2060
474 compared with 2001-2010, much higher than the change of 66% in Yue et al. (2015). In
475 contrast, Amiro et al. (2009) predicted that boreal area burned at the $2\times CO_2$ scenario
476 increases only by 34% relative to the $1\times CO_2$ scenario. This ratio is only half of the estimate
477 in Yue et al. (2015), which compared results between periods with $1.44\times CO_2$ and $1\times CO_2$.
478 The discrepancies among these studies are more likely attributed to the differences in fire
479 models. Although both Amiro et al. (2009) and Yue et al. (2015) developed fire-weather
480 regressions in boreal ecoregions, the former study did not include geopotential height at 500
481 hPa and surface relative humidity as predictors, which make dominant contributions to area
482 burned changes in the latter study. On the other hand, Balshi et al. (2009) developed
483 nonlinear regressions between area burned and climate at grid scale, which helps retain
484 extreme values at both the temporal and spatial domain. Compared to previous estimates,
485 Yue et al. (2015) predicted median increases in future fire emissions over boreal North
486 America.
487

Predicted surface [O_3] is much higher than observations over boreal North America (Fig. 3). This bias does not affect main conclusions of this study, because predicted O_3 causes limited damages to boreal GPP even with the overestimated [O_3] (Fig. 5). The result confirms that fire-induced O_3 vegetation damage is negligible in boreal North America. For aerosols, the model captures reasonable spatial pattern of AOD but with a background value of ~0.1 outside fire-prone regions, where the actual AOD is usually 0.1-0.2 (Fig. 2). This discrepancy may be related to the insufficient representations of physical and chemical processes in the model, but may also result from the retrieval biases in MODIS data due to the poor surface conditions (Liu et al., 2005) and small AOD variations (Vachon et al., 2004) at high latitudes.

Simulated aerosol climatic effects depend on radiative and physical processes implemented in the climate model. We find that present-day boreal fire aerosols on average absorb 1.5 W m^{-2} in the atmosphere (Fig. 6), which is much smaller than the value of 20.5 ± 9.3 W m^{-2} for fires in equatorial Asia (Tosca et al., 2010). This is because boreal fires enhance AOD only by 0.03 while tropical fires increase AOD by ~0.4. Previous modeling studies showed that fire plumes induce regional and downwind drought through enhanced atmospheric stability (Feingold et al., 2005; Tosca et al., 2010; Liu et al., 2014). Most of these results were based on the direct and/or semi-direct radiative effects of fire aerosols. Inclusion of the indirect aerosol effect may further inhibit precipitation and amplify drought, but may also introduce additional uncertainties for the simulations. The fire-drought interaction may promote fire activity, especially in a warmer climate. Ignoring this interaction may underestimate future area burned and the consequent emissions.

4.3 Implications

Inverse modeling studies have shown that the land ecosystems of boreal North America are carbon neutral in the present day, with the estimated land-to-air carbon flux from -270 ± 130 Tg C yr^{-1} to 300 ± 500 Tg C yr^{-1} (Gurney et al., 2002; Rodenbeck et al., 2003; Baker et al., 2006; Jacobson et al., 2007; Deng et al., 2014). Here, we reveal a missing land carbon source due to future wildfire pollution, taking into account full coupling among fire activity, climate change, air pollution, and the carbon cycle. Fire pollution aerosol increases boreal NPP by 72 Tg C yr^{-1} in the present day, comparable to the direct carbon loss of 68 Tg C yr^{-1} from wildfire CO_2 emissions. By midcentury, increasing fire emissions instead cause a NPP reduction of 118 Tg C yr^{-1} due to the amplified drought. Although NPP is not a direct

indicator of the land carbon sink, reduction of NPP is always accompanied with the decline of net ecosystem exchange (NEE) and the enhanced carbon loss. In combination with the enhanced carbon emission of 130 Tg C yr^{-1}, future boreal wildfire presents an increasing threat to the regional carbon balance and global warming mitigation. Furthermore, the NPP reductions are mostly located in southern Canada, where cropland is the dominant ecosystem, newly exposing the future wildfire-related air pollution risk to food production.

Acknowledgements. Xu Yue acknowledges funding support from the National Basic Research Program of China (973 program, Grant No. 2014CB441202) and the "Thousand Youth Talents Plan". Nadine Unger acknowledges funding support from The University of Exeter.

Reference

Alvarado, M. J., Logan, J. A., Mao, J., Apel, E., Riemer, D., Blake, D., Cohen, R. C., Min, K. E., Perring, A. E., Browne, E. C., Wooldridge, P. J., Diskin, G. S., Sachse, G. W., Fuelberg, H., Sessions, W. R., Harrigan, D. L., Huey, G., Liao, J., Case-Hanks, A., Jimenez, J. L., Cubison, M. J., Vay, S. A., Weinheimer, A. J., Knapp, D. J., Montzka, D. D., Flocke, F. M., Pollack, I. B., Wennberg, P. O., Kurten, A., Crounse, J., St Clair, J. M., Wisthaler, A., Mikoviny, T., Yantosca, R. M., Carouge, C. C., and Le Sager, P.: Nitrogen oxides and PAN in plumes from boreal fires during ARCTAS-B and their impact on ozone: an integrated analysis of aircraft and satellite observations, Atmospheric Chemistry and Physics, 10, 9739-9760, doi:10.5194/Acp-10-9739-2010, 2010.

Amiro, B. D., Cantin, A., Flannigan, M. D., and de Groot, W. J.: Future emissions from Canadian boreal forest fires, Canadian Journal of Forest Research, 39, 383-395, doi:10.1139/X08-154, 2009.

Andreae, M. O., and Merlet, P.: Emission of trace gases and aerosols from biomass burning, Global Biogeochemical Cycles, 15, 955-966, 2001.

Atkin, O. K., and Tjoelker, M. G.: Thermal acclimation and the dynamic response of plant respiration to temperature, Trends in Plant Science, 8, 343-351, doi:10.1016/S1360-1385(03)00136-5, 2003.

Baker, D. F., Law, R. M., Gurney, K. R., Rayner, P., Peylin, P., Denning, A. S., Bousquet, P., Bruhwiler, L., Chen, Y. H., Ciais, P., Fung, I. Y., Heimann, M., John, J., Maki, T., Maksyutov, S., Masarie, K., Prather, M., Pak, B., Taguchi, S., and Zhu, Z.: TransCom 3 inversion intercomparison: Impact of transport model errors on the interannual variability of regional CO2 fluxes, 1988-2003, Global Biogeochemical Cycles, 20, Gb1002, doi:10.1029/2004gb002439, 2006.

Ball, J. T., Woodrow, I. E., and Berry, J. A.: A model predicting stomatal conductance and its contribution to the control of photosyn- thesis under different environmental conditions, in: Progress in Photosynthesis Research, edited by: Biggins, J., Nijhoff, Dordrecht, Netherlands, 110–112, 1987.

Balshi, M. S., McGuirez, A. D., Duffy, P., Flannigan, M., Walsh, J., and Melillo, J.: Assessing the response of area burned to changing climate in western boreal North America using a Multivariate Adaptive Regression Splines (MARS) approach, Global Change Biology, 15, 578-600, doi:10.1111/J.1365-2486.2008.01679.X, 2009.

Beer, C., Reichstein, M., Tomelleri, E., Ciais, P., Jung, M., Carvalhais, N., Rodenbeck, C., Arain, M. A., Baldocchi, D., Bonan, G. B., Bondeau, A., Cescatti, A., Lasslop, G., Lindroth, A., Lomas, M., Luyssaert, S., Margolis, H., Oleson, K. W., Roupsard, O., Veenendaal, E., Viovy, N., Williams, C., Woodward, F. I., and Papale, D.: Terrestrial Gross Carbon Dioxide Uptake: Global Distribution and Covariation with Climate, Science, 329, 834-838, doi:10.1126/Science.1184984, 2010.

Bergeron, Y., Cyr, D., Girardin, M. P., and Carcaillet, C.: Will climate change drive 21st century burn rates in Canadian boreal forest outside of its natural variability: collating global climate model experiments with sedimentary charcoal data, International Journal of Wildland Fire, 19, 1127-1139, doi:10.1071/Wf09092, 2010.

Bond-Lamberty, B., Peckham, S. D., Ahl, D. E., and Gower, S. T.: Fire as the dominant driver of central Canadian boreal forest carbon balance, Nature, 450, 89-92, doi:10.1038/Nature06272, 2007.

Chen, L., Huang, J.-G., Alam, S. A., Zhai, L., Dawson, A., Stadt, K. J., and Comeau, P. G.: Drought causes reduced growth of trembling aspen in western Canada, Global Change Biology, in press, doi:10.1111/gcb.13595, 2017.

584 Cirino, G. G., Souza, R. A. F., Adams, D. K., and Artaxo, P.: The effect of atmospheric
585 aerosol particles and clouds on net ecosystem exchange in the Amazon, Atmospheric
586 Chemistry and Physics, 14, 6523-6543, doi:10.5194/acp-14-6523-2014, 2014.
587 Cohan, D. S., Xu, J., Greenwald, R., Bergin, M. H., and Chameides, W. L.: Impact of
588 atmospheric aerosol light scattering and absorption on terrestrial net primary productivity,
589 Global Biogeochemical Cycles, 16, 1090, doi:10.1029/2001gb001441, 2002.
590 Cook, B. I., Miller, R. L., and Seager, R.: Amplification of the North American “Dust Bowl”
591 drought through human-induced land degradation, Proceedings of the National Academy
592 of Sciences of the United States of America, 106, 4997-5001,
593 doi:10.1073/pnas.0810200106, 2009.
594 Cox, P. M.: Description of the "TRIFFID" Dynamic Global Vegetation Model, Hadley
595 Centre technical note 24, 2001.
596 de Groot, W. J., Flannigan, M. D., and Cantin, A. S.: Climate change impacts on future
597 boreal fire regimes, Forest Ecology and Management, 294, 35-44,
598 doi:10.1016/j.foreco.2012.09.027, 2013.
599 Deng, F., Jones, D. B. A., Henze, D. K., Bousserez, N., Bowman, K. W., Fisher, J. B., Nassar,
600 R., O'Dell, C., Wunch, D., Wennberg, P. O., Kort, E. A., Wofsy, S. C., Blumenstock, T.,
601 Deutscher, N. M., Griffith, D. W. T., Hase, F., Heikkinen, P., Sherlock, V., Strong, K.,
602 Sussmann, R., and Warneke, T.: Inferring regional sources and sinks of atmospheric
603 CO2 from GOSAT XCO2 data, Atmospheric Chemistry and Physics, 14, 3703-3727,
604 doi:10.5194/acp-14-3703-2014, 2014.
605 Duffy, P. A., Walsh, J. E., Graham, J. M., Mann, D. H., and Rupp, T. S.: Impacts of large-
606 scale atmospheric-ocean variability on Alaskan fire season severity, Ecological
607 Applications, 15, 1317-1330, doi:Doi 10.1890/04-0739, 2005.
608 Farquhar, G. D., Caemmerer, S. V., and Berry, J. A.: A Biochemical-Model of
609 Photosynthetic Co2 Assimilation in Leaves of C-3 Species, Planta, 149, 78-90,
610 doi:10.1007/Bf00386231, 1980.
611 Feingold, G., Jiang, H., and Harrington, J. Y.: On smoke suppression of clouds in Amazonia,
612 Geophysical Research Letters, 32, L02804, doi:10.1029/2004GL021369, 2005.
613 Flannigan, M. D., Logan, K. A., Amiro, B. D., Skinner, W. R., and Stocks, B. J.: Future area
614 burned in Canada, Climatic Change, 72, 1-16, doi:10.1007/S10584-005-5935-Y, 2005.
615 Gillett, N. P., Weaver, A. J., Zwiers, F. W., and Flannigan, M. D.: Detecting the effect of
616 climate change on Canadian forest fires, Geophysical Research Letters, 31, L18211,
617 doi:10.1029/2004gl020876, 2004.
618 Girardin, M. P., and Mudelsee, M.: Past and future changes in Canadian boreal wildfire
619 activity, Ecological Applications, 18, 391-406, doi:Doi 10.1890/07-0747.1, 2008.
620 Girardin, M. P., Hogg, E. H., Bernier, P. Y., Kurz, W. A., Guo, X. J., and Cyr, G.: Negative
621 impacts of high temperatures on growth of black spruce forests intensify with the
622 anticipated climate warming, Global Change Biology, 22, 627-643,
623 doi:10.1111/gcb.13072, 2016.
624 Gurney, K. R., Law, R. M., Denning, A. S., Rayner, P. J., Baker, D., Bousquet, P., Bruhwiler,
625 L., Chen, Y. H., Ciais, P., Fan, S., Fung, I. Y., Gloor, M., Heimann, M., Higuchi, K.,
626 John, J., Maki, T., Maksyutov, S., Masarie, K., Peylin, P., Prather, M., Pak, B. C.,
627 Randerson, J., Sarmiento, J., Taguchi, S., Takahashi, T., and Yuen, C. W.: Towards
628 robust regional estimates of CO2 sources and sinks using atmospheric transport models,
629 Nature, 415, 626-630, doi:10.1038/415626a, 2002.
630 Hansen, M. C., DeFries, R. S., Townshend, J. R. G., Carroll, M., Dimiceli, C., and Sohlberg,
631 R. A.: Global Percent Tree Cover at a Spatial Resolution of 500 Meters: First Results of
632 the MODIS Vegetation Continuous Fields Algorithm, Earth Interactions, 7, 1-15,
633 doi:10.1175/1087-3562(2003)007<0001:GPTCAA>2.0.CO;2, 2003.

634 Jacobson, A. R., Fletcher, S. E. M., Gruber, N., Sarmiento, J. L., and Gloor, M.: A joint
635 atmosphere-ocean inversion for surface fluxes of carbon dioxide: 2. Regional results,
636 Global Biogeochemical Cycles, 21, Gb1020, doi:10.1029/2006gb002703, 2007.
637 Jung, M., Reichstein, M., and Bondeau, A.: Towards global empirical upscaling of
638 FLUXNET eddy covariance observations: validation of a model tree ensemble approach
639 using a biosphere model, Biogeosciences, 6, 2001-2013, doi:10.5194/bg-6-2001-2009,
640 2009.
641 Kanniah, K. D., Beringer, J., North, P., and Hutley, L.: Control of atmospheric particles on
642 diffuse radiation and terrestrial plant productivity: A review, Progress in Physical
643 Geography, 36, 209-237, doi:10.1177/0309133311434244, 2012.
644 Kasischke, E. S., and Turetsky, M. R.: Recent changes in the fire regime across the North
645 American boreal region - Spatial and temporal patterns of burning across Canada and
646 Alaska, Geophysical Research Letters, 33, doi:10.1029/2006gl025677, 2006.
647 Levy, R. C., Mattoo, S., Munchak, L. A., Remer, L. A., Sayer, A. M., Patadia, F., and Hsu, N.
648 C.: The Collection 6 MODIS aerosol products over land and ocean, Atmospheric
649 Measurement Techniques, 6, 2989-3034, doi:10.5194/amt-6-2989-2013, 2013.
650 Liu, H. Q., Pinker, R. T., and Holben, B. N.: A global view of aerosols from merged transport
651 models, satellite, and ground observations, J. Geophys. Res., 110, -, 2005.
652 Liu, J. C., Wilson, A., Mickley, L. J., Ebisu, K., Wang, Y., Sulprizio, M. P., Peng, R. D., Yue,
653 X., Son, J.-Y., Anderson, G. B., Dominici, F., and Bell, M. L.: Wildfire-specific Fine
654 Particulate Matter and Risk of Hospital Admissions in Urban and Rural Counties,
655 Epidemiology, 28, 77-85, doi:10.1097/EDE.0000000000000556, 2017.
656 Liu, Y.: Enhancement of the 1988 northern U.S. drought due to wildfires, Geophysical
657 Research Letters, 32, L10806, doi:10.1029/2005GL022411, 2005.
658 Liu, Y., Goodrick, S., and Heilman, W.: Wildland fire emissions, carbon, and climate:
659 Wildfire–climate interactions, Forest Ecology and Management, 317, 80-96,
660 doi:10.1016/j.foreco.2013.02.020, 2014.
661 Ma, Z. H., Peng, C. H., Zhu, Q. A., Chen, H., Yu, G. R., Li, W. Z., Zhou, X. L., Wang, W. F.,
662 and Zhang, W. H.: Regional drought-induced reduction in the biomass carbon sink of
663 Canada's boreal forests, Proceedings of the National Academy of Sciences of the United
664 States of America, 109, 2423-2427, doi:10.1073/pnas.1111576109, 2012.
665 McKenzie, D., Raymond, C. L., Kellogg, L. K. B., Norheim, R. A., Andreu, A. G., Bayard, A.
666 C., Kopper, K. E., and Elman, E.: Mapping fuels at multiple scales: landscape
667 application of the Fuel Characteristic Classification System, Canadian Journal of Forest
668 Research, 37, 2421-2437, doi:10.1139/X07-056, 2007.
669 Meehl, G. A., Covey, C., Delworth, T., Latif, M., McAvaney, B., Mitchell, J. F. B., Stouffer,
670 R. J., and Taylor, K. E.: The WCRP CMIP3 multi-model dataset: A new era in climate
671 change research, Bulletin of the American Meteorological Society, 88, 1383-1394,
672 doi:10.1175/BAMS-88-9-1383, 2007.
673 Morris, G. A., Hersey, S., Thompson, A. M., Pawson, S., Nielsen, J. E., Colarco, P. R.,
674 McMillan, W. W., Stohl, A., Turquety, S., Warner, J., Johnson, B. J., Kucsera, T. L.,
675 Larko, D. E., Oltmans, S. J., and Witte, J. C.: Alaskan and Canadian forest fires
676 exacerbate ozone pollution over Houston, Texas, on 19 and 20 July 2004, Journal of
677 Geophysical Research, 111, D24s03, doi:10.1029/2006jd007090, 2006.
678 Munchak, L. A., Levy, R. C., Mattoo, S., Remer, L. A., Holben, B. N., Schafer, J. S.,
679 Hostetler, C. A., and Ferrare, R. A.: MODIS 3 km aerosol product: applications over
680 land in an urban/suburban region, Atmospheric Measurement Techniques, 6, 1747-1759,
681 doi:10.5194/amt-6-1747-2013, 2013.

682 Nadeau, L. B., McRae, D. J., and Jin, J. Z.: Development of a national fuel-type map for
683 Canada using fuzzy logic, Natural Resources Canada, Canadian Forest Service, Northern
684 Forestry Centre, Edmonton, Alberta.Information Report NOR-X-406, 2005.
685 Nitschke, C. R., and Innes, J. L.: Climatic change and fire potential in South-Central British
686 Columbia, Canada, Global Change Biology, 14, 841-855, doi:10.1111/j.1365-
687 2486.2007.01517.x, 2008.
688 Niyogi, D., Chang, H.-I., Saxena, V. K., Holt, T., Alapaty, K., Booker, F., Chen, F., Davis, K.
689 J., Holben, B., Matsui, T., Meyers, T., Oechel, W. C., Sr., R. A. P., Wells, R., Wilson, K.,
690 and Xue, Y.: Direct observations of the effects of aerosol loading on net ecosystem CO 2
691 exchanges over different landscapes, Geophysical Research Letters, 31,
692 doi:10.1029/2004GL020915, 2004.
693 Oleson, K. W., Lawrence, D. M., Bonan, G. B., Flanne, M. G., Kluzek, E., Lawrence, P. J.,
694 Levis, S., Swenson, S. C., and Thornton, P. E.: Technical Description of version 4.0 of
695 the Community Land Model (CLM), National Center for Atmospheric Research,
696 Boulder, CONCAR/TN-478+STR, 2010.
697 Oliveira, P. H. F., Artaxo, P., Pires, C., de Lucca, S., Procópio, A., Holben, B., Schafer, J.,
698 Cardoso, L. F., Wofsy, S. C., and Rocha, H. R.: The effects of biomass burning aerosols
699 and clouds on the CO2 flux in Amazonia, Tellus Series B-Chemical and Physical
700 Meteorology, 59, 338-349, doi:10.1111/j.1600-0889.2007.00270.x, 2007.
701 Pacifico, F., Folberth, G. A., Sitch, S., Haywood, J. M., Rizzo, L. V., Malavelle, F. F., and
702 Artaxo, P.: Biomass burning related ozone damage on vegetation over the Amazon forest:
703 a model sensitivity study, Atmospheric Chemistry and Physics, 15, 2791-2804,
704 doi:10.5194/acp-15-2791-2015, 2015.
705 Randerson, J. T., Liu, H., Flanner, M. G., Chambers, S. D., Jin, Y., Hess, P. G., Pfister, G.,
706 Mack, M. C., Treseder, K. K., Welp, L. R., Chapin, F. S., Harden, J. W., Goulden, M. L.,
707 Lyons, E., Neff, J. C., Schuur, E. A. G., and Zender, C. S.: The impact of boreal forest
708 fire on climate warming, Science, 314, 1130-1132, doi:10.1126/Science.1132075, 2006.
709 Rap, A., Spracklen, D. V., Mercado, L., Reddington, C. L., Haywood, J. M., Ellis, R. J.,
710 Phillips, O. L., Artaxo, P., Bonal, D., Coupe, N. R., and Butt, N.: Fires increase Amazon
711 forest productivity through increases in diffuse radiation, Geophysical Research Letters,
712 42, 4654-4662, doi:10.1002/2015gl063719, 2015.
713 Remer, L. A., Mattoo, S., Levy, R. C., and Munchak, L. A.: MODIS 3 km aerosol product:
714 algorithm and global perspective, Atmospheric Measurement Techniques, 6, 1829-1844,
715 doi:10.5194/amt-6-1829-2013, 2013.
716 Rodenbeck, C., Houweling, S., Gloor, M., and Heimann, M.: CO2 flux history 1982-2001
717 inferred from atmospheric data using a global inversion of atmospheric transport,
718 Atmospheric Chemistry and Physics, 3, 1919-1964, 2003.
719 Schaefer, K., Collatz, G. J., Tans, P., Denning, A. S., Baker, I., Berry, J., Prihodko, L., Suits,
720 N., and Philpott, A.: Combined Simple Biosphere/Carnegie-Ames-Stanford Approach
721 terrestrial carbon cycle model, J. Geophys. Res., 113, G03034,
722 doi:10.1029/2007jg000603, 2008.
723 Schmidt, G. A., Kelley, M., Nazarenko, L., Ruedy, R., Russell, G. L., Aleinov, I., Bauer, M.,
724 Bauer, S. E., Bhat, M. K., Bleck, R., Canuto, V., Chen, Y. H., Cheng, Y., Clune, T. L.,
725 Del Genio, A., de Fainchtein, R., Faluvegi, G., Hansen, J. E., Healy, R. J., Kiang, N. Y.,
726 Koch, D., Lacis, A. A., LeGrande, A. N., Lerner, J., Lo, K. K., Matthews, E. E., Menon,
727 S., Miller, R. L., Oinas, V., Oloso, A. O., Perlwitz, J. P., Puma, M. J., Putman, W. M.,
728 Rind, D., Romanou, A., Sato, M., Shindell, D. T., Sun, S., Syed, R. A., Tausnev, N.,
729 Tsigaridis, K., Unger, N., Voulgarakis, A., Yao, M. S., and Zhang, J. L.: Configuration
730 and assessment of the GISS ModelE2 contributions to the CMIP5 archive, Journal of
731 Advances in Modeling Earth Systems, 6, 141-184, doi:10.1002/2013ms000265, 2014.

Shindell, D. T., Lamarque, J. F., Schulz, M., Flanner, M., Jiao, C., Chin, M., Young, P. J., Lee, Y. H., Rotstayn, L., Mahowald, N., Milly, G., Faluvegi, G., Balkanski, Y., Collins, W. J., Conley, A. J., Dalsoren, S., Easter, R., Ghan, S., Horowitz, L., Liu, X., Myhre, G., Nagashima, T., Naik, V., Rumbold, S. T., Skeie, R., Sudo, K., Szopa, S., Takemura, T., Voulgarakis, A., Yoon, J. H., and Lo, F.: Radiative forcing in the ACCMIP historical and future climate simulations, Atmospheric Chemistry and Physics, 13, 2939-2974, doi:Doi 10.5194/Acp-13-2939-2013, 2013a.

Shindell, D. T., Pechony, O., Voulgarakis, A., Faluvegi, G., Nazarenko, L., Lamarque, J. F., Bowman, K., Milly, G., Kovari, B., Ruedy, R., and Schmidt, G. A.: Interactive ozone and methane chemistry in GISS-E2 historical and future climate simulations, Atmospheric Chemistry and Physics, 13, 2653-2689, doi:10.5194/Acp-13-2653-2013, 2013b.

Sitch, S., Cox, P. M., Collins, W. J., and Huntingford, C.: Indirect radiative forcing of climate change through ozone effects on the land-carbon sink, Nature, 448, 791-794, doi:10.1038/Nature06059, 2007.

Solomon, S., Qin, D., Manning, M., Chen, Z., Marquis, M., Averyt, K. B., Tignor, M., and Miller, H. L.: Climate Change 2007: Working Group I: The Physical Science Basis, Cambridge University Press, Cambridge, United Kingdom and New York, NY, USA, 2007.

Spitters, C. J. T.: Separating the Diffuse and Direct Component of Global Radiation and Its Implications for Modeling Canopy Photosynthesis .2. Calculation of Canopy Photosynthesis, Agricultural and Forest Meteorology, 38, 231-242, doi:10.1016/0168-1923(86)90061-4, 1986.

Stocks, B. J., Mason, J. A., Todd, J. B., Bosch, E. M., Wotton, B. M., Amiro, B. D., Flannigan, M. D., Hirsch, K. G., Logan, K. A., Martell, D. L., and Skinner, W. R.: Large forest fires in Canada, 1959-1997, Journal of Geophysical Research, 108, 8149, doi:10.1029/2001jd000484, 2002.

Strada, S., Unger, N., and Yue, X.: Observed aerosol-induced radiative effect on plant productivity in the eastern United States, Atmospheric Environment, 122, 463–476, doi:10.1016/j.atmosenv.2015.09.051, 2015.

Tosca, M. G., Randerson, J. T., Zender, C. S., Flanner, M. G., and Rasch, P. J.: Do biomass burning aerosols intensify drought in equatorial Asia during El Nin˜o?, Atmospheric Chemistry and Physics, 10, 3515-3528, doi:10.5194/acp-10-3515-2010, 2010.

Turetsky, M. R., Kane, E. S., Harden, J. W., Ottmar, R. D., Manies, K. L., Hoy, E., and Kasischke, E. S.: Recent acceleration of biomass burning and carbon losses in Alaskan forests and peatlands, Nature Geoscience, 4, 27-31, doi:10.1038/Ngeo1027, 2011.

Tymstra, C., Flannigan, M. D., Armitage, O. B., and Logan, K.: Impact of climate change on area burned in Alberta's boreal forest, International Journal of Wildland Fire, 16, 153-160, doi:10.1071/Wf06084, 2007.

Unger, N., Harper, K., Zheng, Y., Kiang, N. Y., Aleinov, I., Arneth, A., Schurgers, G., Amelynck, C., Goldstein, A., Guenther, A., Heinesch, B., Hewitt, C. N., Karl, T., Laffineur, Q., Langford, B., McKinney, K. A., Misztal, P., Potosnak, M., Rinne, J., Pressley, S., Schoon, N., and Serça, D.: Photosynthesis-dependent isoprene emission from leaf to planet in a global carbon–chemistry–climate model, Atmos. Chem. Phys., 13, 17717-17791, doi:10.5194/acp-13-10243-2013, 2013.

Vachon, F., Royer, A., Aube, M., Toubbe, B., O'Neill, N. T., and Teillet, P. M.: Remote sensing of aerosols over North American land surfaces from POLDER and MODIS measurements, Atmospheric Environment, 38, 3501-3515, doi:10.1016/j.atmosenv.2004.01.046, 2004.

781 Val Martin, M., Kahn, R. A., Logan, J. A., Paugam, R., Wooster, M., and Ichoku, C.: Space-
782 based observational constraints for 1-D plume rise models, Journal of Geophysical
783 Research, 117, D22204, doi:10.1029/2012JD018370, 2012.
784 van der Werf, G. R., Randerson, J. T., Giglio, L., Collatz, G. J., Mu, M., Kasibhatla, P. S.,
785 Morton, D. C., DeFries, R. S., Jin, Y., and van Leeuwen, T. T.: Global fire emissions and
786 the contribution of deforestation, savanna, forest, agricultural, and peat fires (1997-2009),
787 Atmospheric Chemistry and Physics, 10, 11707-11735, doi:10.5194/Acp-10-11707-2010,
788 2010.
789 van Vuuren, D. P., Edmonds, J., Kainuma, M., Riahi, K., Thomson, A., Hibbard, K., Hurtt, G.
790 C., Kram, T., Krey, V., Lamarque, J. F., Masui, T., Meinshausen, M., Nakicenovic, N.,
791 Smith, S. J., and Rose, S. K.: The representative concentration pathways: an overview,
792 Climatic Change, 109, 5-31, doi:10.1007/s10584-011-0148-z, 2011.
793 Wang, X. L., Parisien, M. A., Taylor, S. W., Perrakis, D. D. B., Little, J., and Flannigan, M.
794 D.: Future burn probability in south-central British Columbia, International Journal of
795 Wildland Fire, 25, 200-212, doi:10.1071/Wf15091, 2016.
796 Wild, M., Folini, D., Schar, C., Loeb, N., Dutton, E. G., and Konig-Langlo, G.: The global
797 energy balance from a surface perspective, Climate Dynamics, 40, 3107-3134,
798 doi:10.1007/s00382-012-1569-8, 2013.
799 Wotawa, G., and Trainer, M.: The influence of Canadian forest fires on pollutant
800 concentrations in the United States, Science, 288, 324-328, 2000.
801 Wotton, B. M., Nock, C. A., and Flannigan, M. D.: Forest fire occurrence and climate change
802 in Canada, International Journal of Wildland Fire, 19, 253-271, doi:10.1071/Wf09002,
803 2010.
804 Yue, X., Mickley, L. J., Logan, J. A., and Kaplan, J. O.: Ensemble projections of wildfire
805 activity and carbonaceous aerosol concentrations over the western United States in the
806 mid-21st century, Atmos. Environ., 77, 767-780, doi:10.1016/J.Atmosenv.2013.06.003,
807 2013.
808 Yue, X., and Unger, N.: Ozone vegetation damage effects on gross primary productivity in
809 the United States, Atmospheric Chemistry and Physics, 14, 9137-9153, doi:10.5194/acp-
810 14-9137-2014, 2014.
811 Yue, X., Mickley, L. J., Logan, J. A., Hudman, R. C., Martin, M. V., and Yantosca, R. M.:
812 Impact of 2050 climate change on North American wildfire: consequences for ozone air
813 quality, Atmospheric Chemistry and Physics, 15, 10033-10055, doi:10.5194/acp-15-
814 10033-2015, 2015.
815 Yue, X., and Unger, N.: The Yale Interactive terrestrial Biosphere model version 1.0:
816 description, evaluation and implementation into NASA GISS ModelE2, Geoscientific
817 Model Development, 8, 2399-2417, doi:10.5194/gmd-8-2399-2015, 2015.
818 Yue, X., Keenan, T. F., Munger, W., and Unger, N.: Limited effect of ozone reductions on
819 the 20-year photosynthesis trend at Harvard forest, Global Change Biology, 22, 3750-
820 3759, doi:10.1111/gcb.13300, 2016.
821 Yue, X., Unger, N., Harper, K., Xia, X., Liao, H., Zhu, T., Xiao, J., Feng, Z., and Li, J.:
822 Ozone and haze pollution weakens net primary productivity in China, Atmospheric
823 Chemistry and Physics Discussion, in review, 2017.
824 Zhao, Z., Kooperman, G. J., Pritchard, M. S., Russell, L. M., and Somerville, R. C. J.:
825 Investigating impacts of forest fires in Alaska and western Canada on regional weather
826 over the northeastern United States using CAM5 global simulations to constrain
827 transport to a WRF-Chem regional domain, Journal of Geophysical Research, 119, 7515-
828 7536, doi:10.1002/2013jd020973, 2014.
829 Zu, K., Tao, G., Long, C., Goodman, J., and Valberg, P.: Long-range fine particulate matter
830 from the 2002 Quebec forest fires and daily mortality in Greater Boston and New York

831 City, Air Quality Atmosphere and Health, 9, 213-221, doi:10.1007/s11869-015-0332-9,
832 2016.
833
834

Atmos. Chem. Phys. Discuss., https://doi.org/10.5194/acp-2017-319
Manuscript under review for journal Atmos. Chem. Phys.
Discussion started: 23 June 2017

Atmospheric Chemistry and Physics Discussions

Table 1. Online simulations with ModelE2-YIBs climate model [a]

Simulations	SST	$[CO_2]$	Emissions	Fires	O_3 effect	Aerosol effect
F10O3	2010s	2010s	2010s	2010s	Yes	No
F10AERO	2010s	2010s	2010s	2010s	No	Yes
F10CTRL	2010s	2010s	2010s	No	No	Yes
F50O3	2050s	2050s	2050s	2050s	Yes	No
F50AERO	2050s	2050s	2050s	2050s	No	Yes
F50CTRL	2050s	2050s	2050s	No	No	Yes

[a] Values of SST, $[CO_2]$, and emissions are adopted from RCP8.5 scenario, with the average of 2006-2015 for the 2010s and that of 2046-2055 for the 2050s. For fire emissions, values at the 2010s are predicted based on meteorology for 1981-2000 and those at the 2050s are for 2046-2065.

Atmos. Chem. Phys. Discuss., https://doi.org/10.5194/acp-2017-319
Manuscript under review for journal Atmos. Chem. Phys.
Discussion started: 23 June 2017

Atmospheric Chemistry and Physics Discussions

Table 2. Emissions from wildfires and non-fire sources over boreal North America

Species	Fire emissions (Tg yr^{-1})		Non-fire emissions (Tg yr^{-1})	
	2010s	2050s	2010s	2050s
NO_x [a]	0.39	0.74	2.43	2.08
CO	15.7	28.8	5.9	4.0
SO_2 [a]	0.12	0.22	1.95	1.28
NH_3	0.22	0.40	0.80	1.15
BC	0.08	0.16	0.03	0.01
OC	1.10	2.04	0.04	0.02
NMVOC	0.39	1.34	0.49	0.30
BVOC [b]	N/A	N/A	15.3	15.1

[a] Natural emissions are included for NO_x (lightning and soil) and SO_2 (volcano).
[b] ModelE2-YIBs calculates BVOC emissions using photosynthesis-dependent scheme implemented by Unger et al. (2013).

Atmos. Chem. Phys. Discuss., https://doi.org/10.5194/acp-2017-319
Manuscript under review for journal Atmos. Chem. Phys.
Discussion started: 23 June 2017

Atmospheric Chemistry and Physics Discussions

Table 3. Simulations with YIBs vegetation model driven by offline meteorology from ModelE2-YIBs climate model

Simulations	Base forcing	Temperature	PAR	Soil moisture
Y10_CTRL	F10CTRL			
Y10_ALL	F10CTRL	F10AERO	F10AERO	F10AERO
Y10_TAS	F10CTRL	F10AERO		
Y10_PAR	F10CTRL		F10AERO	
Y10_SLM	F10CTRL			F10AERO
Y50_CTRL	F50CTRL			
Y50_ALL	F50CTRL	F50AERO	F50AERO	F50AERO
Y50_TAS	F50CTRL	F50AERO		
Y50_PAR	F50CTRL		F50AERO	
Y50_SLM	F50CTRL			F50AERO

867
868
869 **Table 4.** Pearson's correlation coefficients for GPP-PAR and GPP-AOD relationships at
870 Ameriflux (AMF) sites [a]
871

Site	Period [b]	Pearson's *R*					
		GPP-PAR	GPP-PAR_{dir}	GPP-PAR_{dif}	GPP-AOD	AOD-PAR_{dif}	AOD-PAR_{dir}
CA-Gro	2004-2013	**0.19** (2432)	-0.01 (2432)	**0.42** (2432)	0.15 (65)	**0.60** (65)	**-0.52** (65)
CA-Qfo	2003-2014	**0.16** (3201)	**-0.04** (3201)	**0.45** (3201)	**0.36** (59)	**0.91** (34)	**-0.80** (34)

872
873 [a] Both GPP and PAR (direct PAR_{dir} and diffuse PAR_{dif}) data are adopted from site-level AMF
874 measurements. AOD data are adopted from instantaneous MODIS Aqua and Terra 3-km
875 retrievals. Correlations are calculated for quasi-coincident AMF and MODIS data over
876 summer noontime (June-August, 10:00-14:00 Local Time). The sampling number for each
877 correlation is denoted in brackets. Significant (p<0.05) correlation coefficients are bolded.
878 [b] For CA-Gro site, diffuse PAR observations of 2005-2009 have been discarded because of
879 poor calibration, as documented on the AMF website.
880
881

Atmos. Chem. Phys. Discuss., https://doi.org/10.5194/acp-2017-319
Manuscript under review for journal Atmos. Chem. Phys.
Discussion started: 23 June 2017

Atmospheric Chemistry and Physics Discussions

882
883
884
885 **Table 5.** Changes in NPP (Tg C yr^{-1}) caused by composite and individual climatic effects of
886 fire aerosols
887

	2010s	2050s
Online [a]	72	-118
Offline total [b]	126	-97
Temperature	11	-22
Radiation	8	14
Soil moisture	104	-86

888
889 [a] Online results are calculated using the ModelE2-YIBs model with (F10AERO – F10CTRL)
890 for the 2010s and (F50AERO – F50CTRL) for the 2050s.
891 [b] Offline results are calculated with the YIBs model driven with individual or combined
892 changes in temperature, radiation, and soil moisture.
893
894
895

Atmos. Chem. Phys. Discuss., https://doi.org/10.5194/acp-2017-319
Manuscript under review for journal Atmos. Chem. Phys.
Discussion started: 23 June 2017

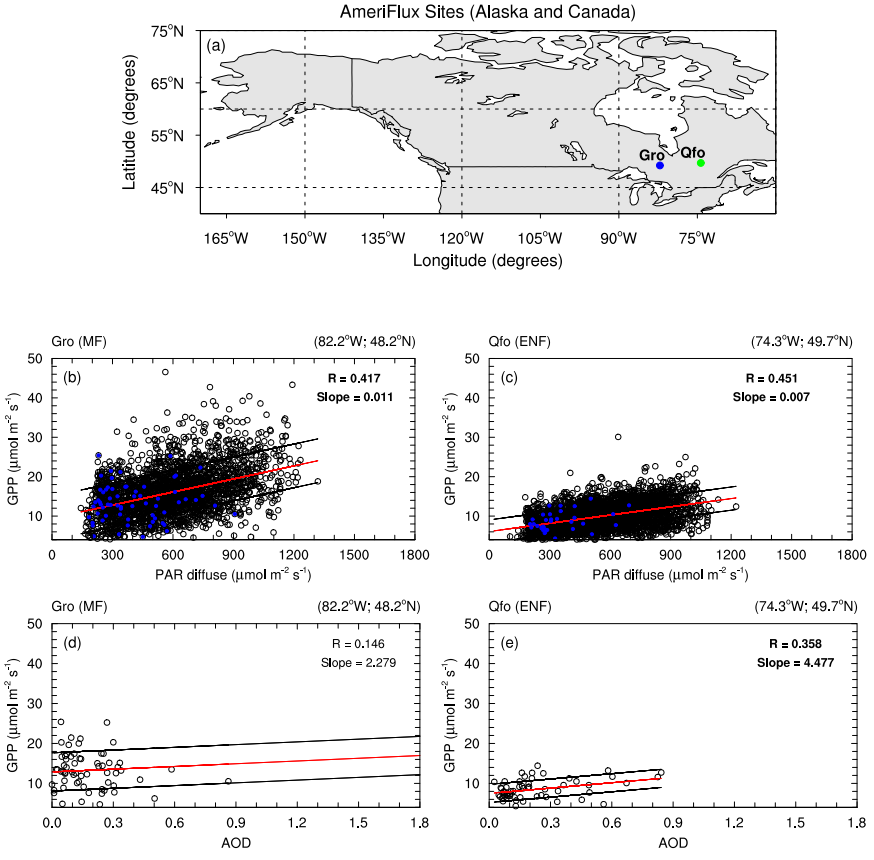

Figure 1. Relationships between (b, c) GPP and diffuse PAR and (d, e) GPP and MODIS AOD at (a) two boreal sites: Groundhog River (Gro) and Quebec Mature Boreal Forest Site (Qfo). The two sites are from the AmeriFlux network in Canada and are dominated by mixed forest (MF at Gro) and evergreen needleleaf forest (ENF at Qfo) (Table 1). Data cover summer days (June-August). AmeriFlux diffuse PAR and GPP (in µmol m^{-2} s^{-1}) are half-hourly observations (10:00-14:00 LT). Instantaneous MODIS Aqua and Terra 3-km AOD are selected in a time span centered on AmeriFlux record time. For each plot: the red line indicates the regression line, black lines depict the 1- σ interval; the regression slope and correlation coefficient are both included for each site (in bold if statistically significant at 95% confidence level). Blue dots in (b, c) show instants when MODIS Aqua and Terra 3-km AODs overlap AmeriFlux data.

Atmos. Chem. Phys. Discuss., https://doi.org/10.5194/acp-2017-319
Manuscript under review for journal Atmos. Chem. Phys.
Discussion started: 23 June 2017

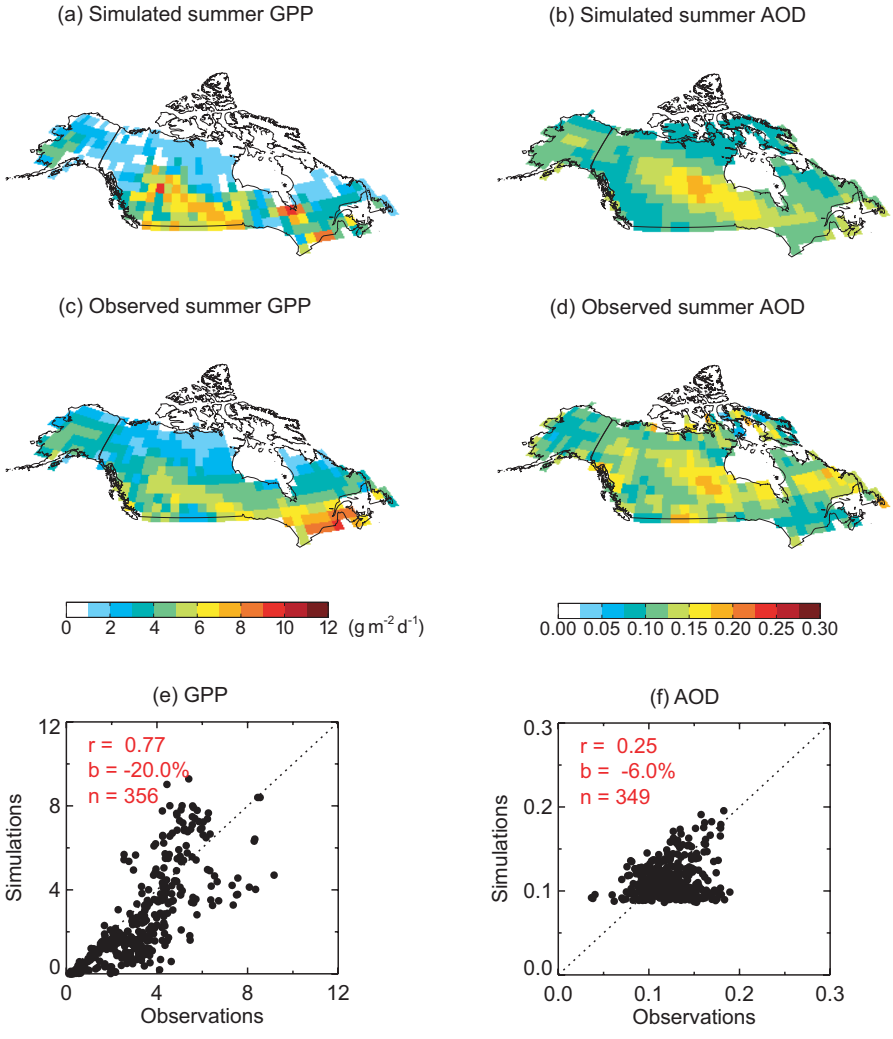

Figure 2. Evaluation of simulated summer (a) GPP and (b) AOD at 550 nm with (c, d) observations. Simulation results are from F10AERO (Table 1). Each point on the (e, f) scatter plot represents one grid square in boreal North America. The number of points (n), correlation coefficient (r), and relative bias (b) for the evaluation are presented on the plot.

Atmos. Chem. Phys. Discuss., https://doi.org/10.5194/acp-2017-319
Manuscript under review for journal Atmos. Chem. Phys.
Discussion started: 23 June 2017

Atmospheric Chemistry and Physics Discussions

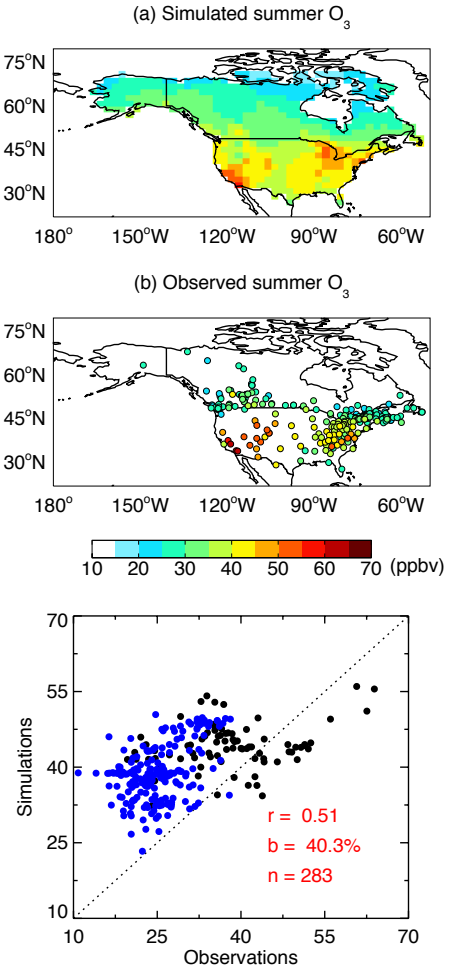

Figure 3. Evaluation of simulated summer surface [O_3] with observations for 2008-2012. Observations are collected from 81 U.S. sites at the Clean Air Status and Trends Network (CASTNET) and 202 Canadian sites at the National Air Pollution Surveillance (NAPS) program. The number of points (n), correlation coefficient (r), and mean bias (b) for the evaluation are presented on the plot. Values over Canada and Alaska are denoted with blue points.

Atmos. Chem. Phys. Discuss., https://doi.org/10.5194/acp-2017-319
Manuscript under review for journal Atmos. Chem. Phys.
Discussion started: 23 June 2017

Atmospheric Chemistry and Physics Discussions

964
965

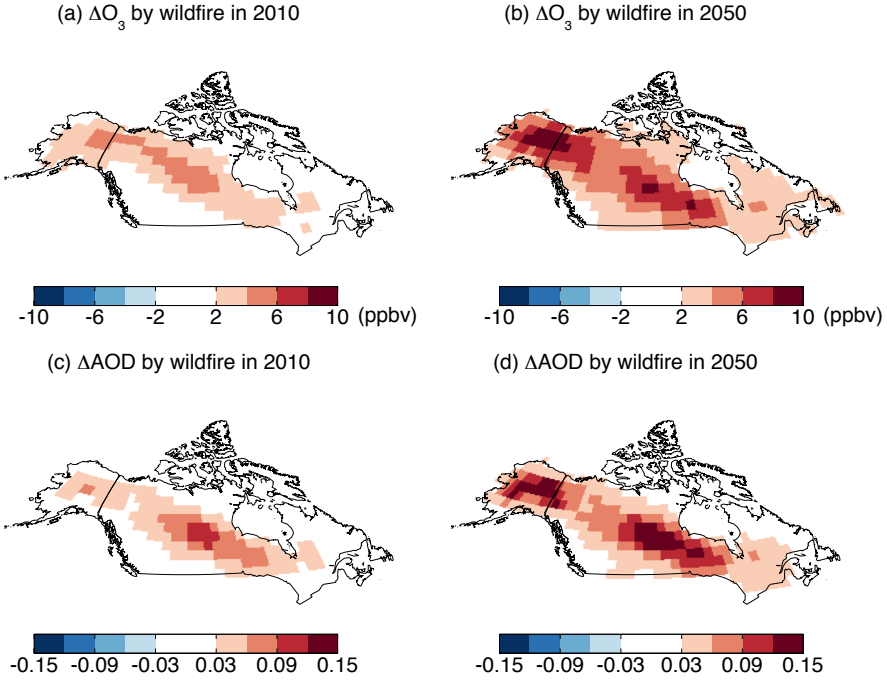

966

967 **Figure 4.** Changes in summer (a, b) [O_3] and (c, d) AOD at 550 nm induced by wildfire
968 emissions in (a, c) the 2010s and (b, d) the 2050s over boreal North America. Only
969 significant changes (p<0.05) are shown.

970

971

Atmos. Chem. Phys. Discuss., https://doi.org/10.5194/acp-2017-319
Manuscript under review for journal Atmos. Chem. Phys.
Discussion started: 23 June 2017

Atmospheric Chemistry and Physics Discussions

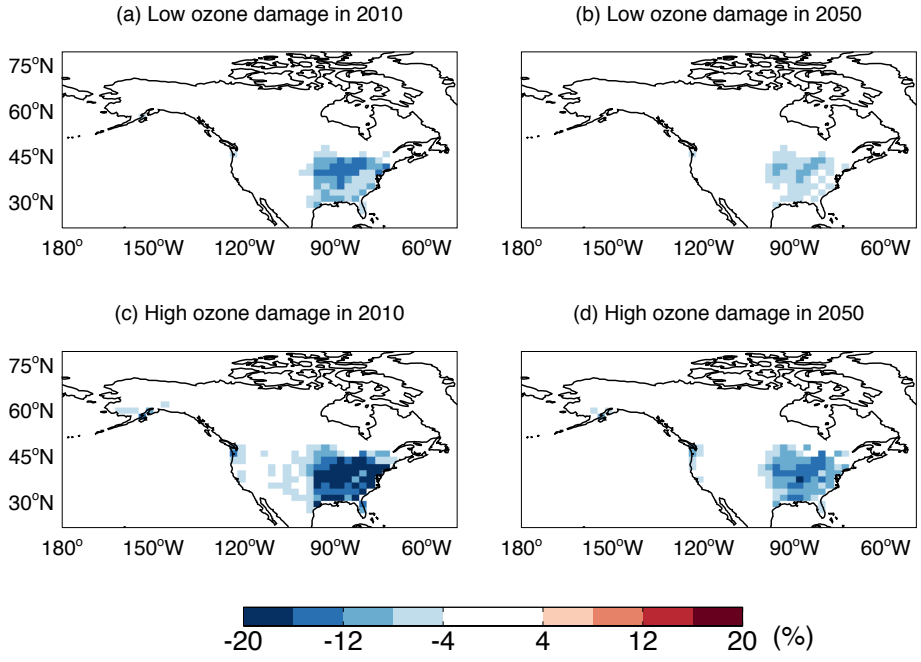

Figure 5. Simulated O_3 damages to summer GPP in North America. Results shown are from simulations with (a, b) low and (c, d) high O_3 sensitivities for (a, c) 2010 and (b, d) 2050. Simulated [O_3] includes contributions from both wildfire and non-fire emissions. Results for 2010 are derived as (F10O3/F10CTRL-1)×100%. Results for 2050 are derived as (F50O3/F50CTRL-1)×100%.

Atmos. Chem. Phys. Discuss., https://doi.org/10.5194/acp-2017-319
Manuscript under review for journal Atmos. Chem. Phys.
Discussion started: 23 June 2017

Atmospheric Chemistry and Physics Discussions

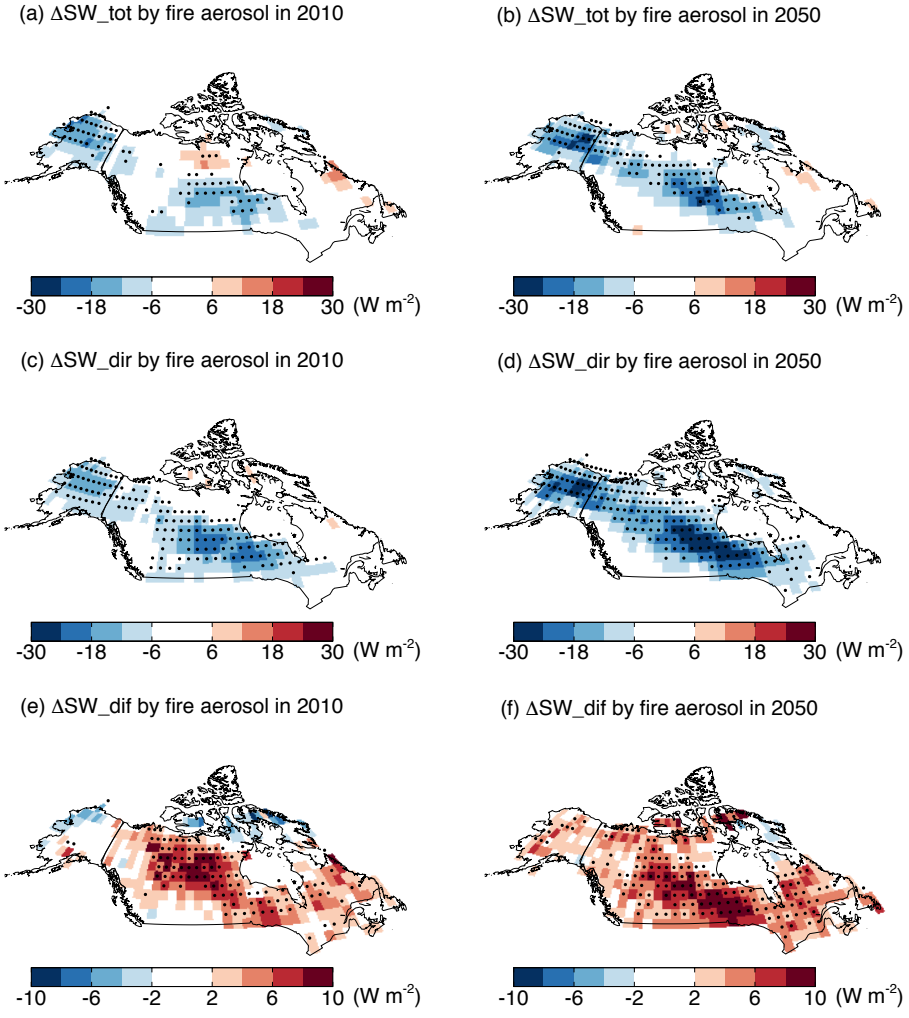

Figure 6. Changes in surface radiative fluxes induced by wildfire aerosols in boreal North America. Results shown are for the changes in summertime (June-August) (a, b) total, (c, d) direct, and (e, f) diffuse solar radiation at surface caused by aerosols from wildfire emissions at (a, c, e) present day and (b, d, f) midcentury. Significant changes (p<0.05) are marked with black dots. Results for 2010 are calculated as (F10AERO - F10CTRL). Results for 2050 are calculated as (F50AERO - F50CTRL).

Atmos. Chem. Phys. Discuss., https://doi.org/10.5194/acp-2017-319
Manuscript under review for journal Atmos. Chem. Phys.
Discussion started: 23 June 2017

Atmospheric Chemistry and Physics Discussions

994
995

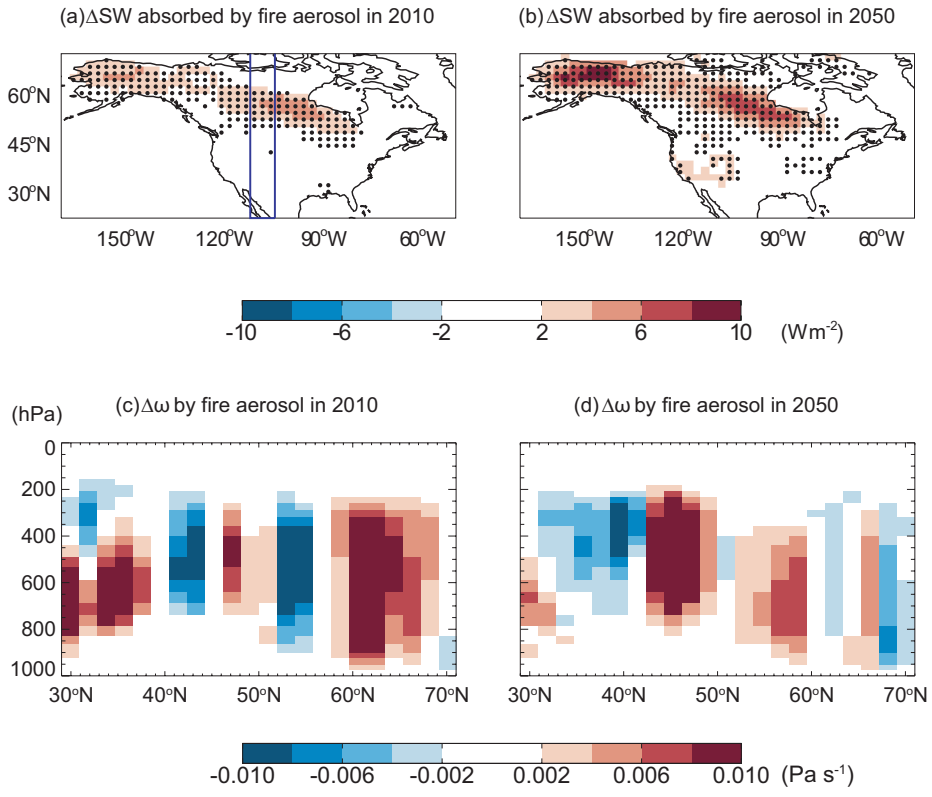

996
997

998 **Figure 7.** Predicted (a, b) absorption of shortwave radiation and (c, d) perturbations in
999 vertical velocity by wildfire aerosols at (a, c) present day and (b, d) midcentury. The
1000 absorption of shortwave radiation is calculated as the differences of radiative perturbations
1001 between top of atmosphere and surface. Vertical velocity is calculated as the longitudinal
1002 average between 105°W and 112.5°W (two blue lines in a). Positive (negative) values
1003 indicate descending (rising) motion. Results for the 2010s are calculated as (F10AERO -
1004 F10CTRL). Results for the 2050s are calculated as (F50AERO - F50CTRL). Significant
1005 changes ($p < 0.05$) in (a, b) are indicated as black points.

1006
1007

Atmos. Chem. Phys. Discuss., https://doi.org/10.5194/acp-2017-319
Manuscript under review for journal Atmos. Chem. Phys.
Discussion started: 23 June 2017

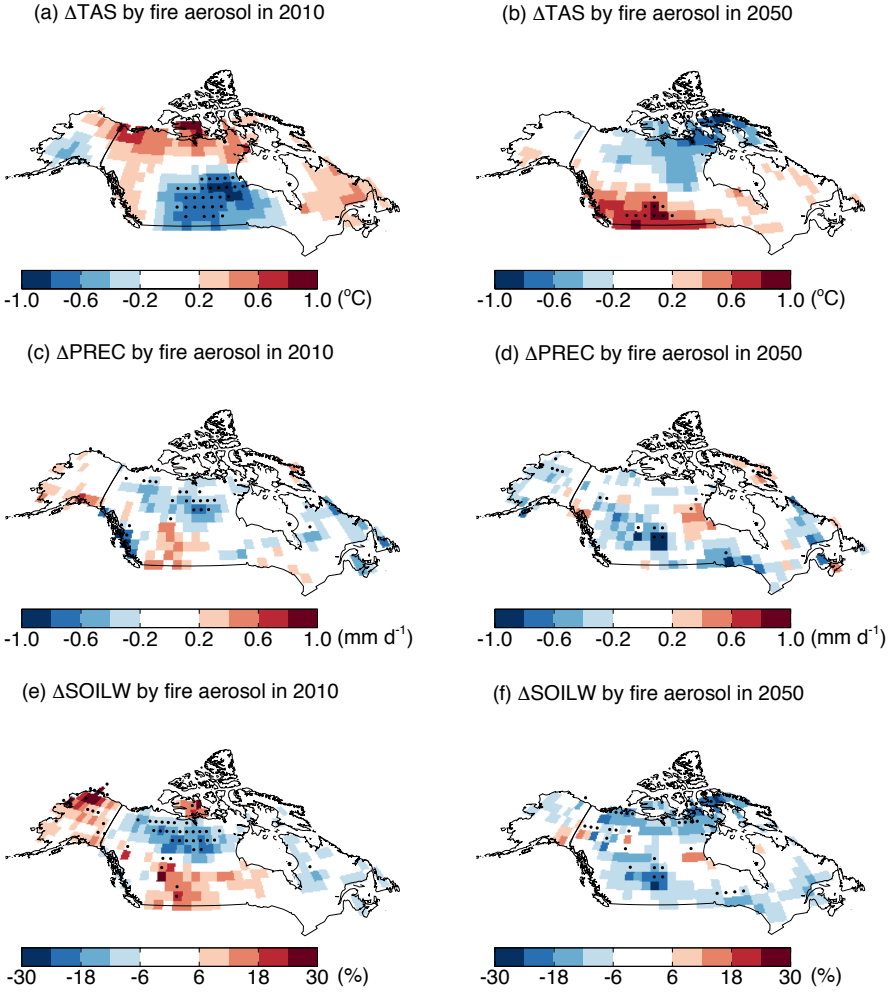

Figure 8. Predicted changes in summertime (a, b) surface air temperature, (c, d) precipitation, and (e, f) soil water content at surface caused by aerosols from wildfire emissions at (a, c, e) present day and (b, d, f) midcentury. Results for temperature and precipitation are shown as absolute changes. Results for soil water are shown as relative changes. Results for the 2010s are calculated as (F10AERO - F10CTRL). Results for the 2050s are calculated as (F50AERO - F50CTRL). Significant changes (p<0.05) are marked with black dots.

Atmos. Chem. Phys. Discuss., https://doi.org/10.5194/acp-2017-319
Manuscript under review for journal Atmos. Chem. Phys.
Discussion started: 23 June 2017

Atmospheric Chemistry and Physics Discussions

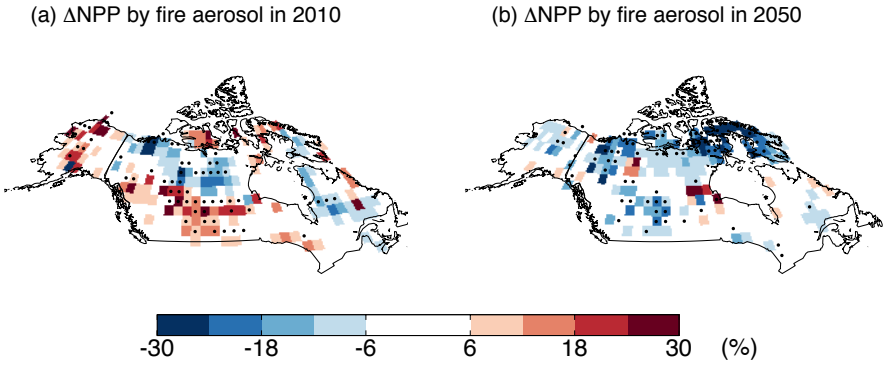

Figure 9. Predicted percentage changes in summer NPP caused by wildfire aerosols at (a) present day and (b) midcentury. Results for the 2010s are calculated as (F10AERO/F10CTRL - 1) × 100%. Results for the 2050s are calculated as (F50AERO/F50CTRL - 1)×100%. Significant changes (p<0.05) are marked with black dots.